Research Article

Chemical Review and Letters
journal homepage: www.chemrevlett.com
ISSN (online): 2645-4947 (print) 2676-7279

Electronic and Magnetic Structure of Monolayer MnAs (111): A case study by DFT

Ahmed Abd Al-Sattar Dawood [1], Abbas Hameed Abdul Hussein[2], Karrar R. Al-Shami[3], Bayan Azizi[4], Rusul Thabit[5], Hebaa M. H[6], Rebaz Obaid kareem[7,] *

[1]*Department of Anesthesia Techniques, Al-Noor University College, Nineveh, Iraq*
[2]*Ahl Al Bayt University Kerbala Iraq*
[3]*College of Science, Department of Forensic Sciences, National University of Science and Technology, Dhi Qar, 64001, Iraq*
[4]*Nursing Department, College of Nursing, University of Human Development, Sulaymaniyah, Kurdistan Region of Iraq*
[5]*Medical technical college, Al-Farahidi University, Iraq*
[6]*Al-Zahrawi University College, Karbala, Iraq*
[7]*Physics Department, College of Science, University of Halabja, 46018, Halabja, Iraq*

ARTICLE INFO

Article history:
Received 13 March 2024
Received in revised form 11 May 2024
Accepted 12 May 2024
Available online 20 May 2024

Keywords:
Density Functional Theory,
Monolayer,
Half-metal,
Magnetic properties.
MnAs (III)

ABSTRACT

We have calculated the electronic and magnetic properties of the monolayer MnAs (111) using a variety of density functional theory (DFT) approaches including PBE-GGA. By cutting the bulk crystalline MnAs in the NiAs-type phase and (111) direction, the properties of this compound have completely changed, and the half-metallic property changes to metallic, and its magnetic properties are increased. The Mn atom has the most effect in creating a stronger magnetic state in the monolayer MnAs (111). In spin up and down, the most electronic states of the Mn atom belong to the valence and the conduction region respectively. The material response to the incident light in the visible light region, as well as the low energy loss in both directions in this region, promises to use it with the lowest range of energy loss in optical applications.

1. Introduction

Recently, the control spin-based electrical currents have opened a new discipline in the electronics industry named Spintronics [1-6]. Half-metals are materials that are suitable candidates in the spintronics industry to increase magnetic memories and application in NMRs and GMRs. [7] These materials are metallic in one spin and semiconductor in the other, with a gap near the Fermi surface. So, these materials are completely magnetic and have a large magnetic polarization near the Fermi surface. Generally, three classes of half-metals named the binary and the full-Heusler, and the half-Heusler compounds are of intense interest [8-10]. Groot *et al* for the first time predicted the half-metallic property in the NiMnSb and PtMnSb Heusler compounds [11,12]. Then other half-metallic Heusler compounds (HM), such as CoMnSi, were studied and synthesized [13-15]. For well-chosen lattice constants, these binary materials have a half-metallic property similar to Heusler compounds. Then, by calculating the crystal's energy in ferromagnetic (FM) and antiferromagnetic structures (AFM), the FM structures of these binary materials [16-18] were found to be more stable [19,20]. In recent years, a lot of theoretical and experimental efforts have been made on these compounds. Compounds like CrTe, MnSb, MnAs, and CrSb [12,15] are generally crystallized in two Zinc-blend and NiAs-type phases. These new half-metals are used to make electronic components, such as transistors, magnetic memories, etc, which is simultaneous with the discovery of tunneling magnetic resistors (TMR) and giant magnetic resistors (GMR) [21,22].

It has been found in recent years that changing material from bulk to layer causes fundamental and basic changes

* Corresponding author: e-mail: obedrebaz9@gmail.com
https://doi.org/10.22034/crl.2024.448436.1312

in the electronic, optical, and even mechanical properties of matter, a prominent example of which is differences in the behavior of graphene compared to graphite structure, and similar situation for graphene-like structures such as Co_2Val and MoS_2 and Cu_2Si, etc [23-30]. The existence of the particular geometric structure that governs single-layer materials, as well as the presence of dangling bonds at their surface, make significant changes in the behavior of these compounds. Therefore, in this study, we established a single-layer structure along (111) direction of the MnAs bulk in the stable phase of NiAs and calculated its structural, electronic, and magnetic properties compared to the bulk structure for the first time.

2. Computational details

In this paper, we used the Wien2K computational software to calculate the physical properties of the crystal [31,32]. In this software, one firstly needs to specify the crystal's atoms, the crystal's structure type, the atomic positions, and desired crystal parameters. We used a 9-atom structure with a lattice constant a = b = 12.182 Bohr, c = 23.04 Bohr, and the lattice angles $\alpha = \beta = 90$ and $\gamma = 118.25$. One of the parameters that is specified in the case.struct file is the radius of the Muffin-tin sphere (RMT), which is chosen to be 2.12Å and 2.23Å for Arsenic and Manganese respectively. To calculate the exchange-correlation energy used in the Cohen-Sham equations, a specific approximation has to be chosen; hence, we used the Perdew-Burke-Ernzerh of generalized gradient approximation (PBE-GGA) approximation for pure MnAs supercell, and then, after optimization the cutoff energy for expanding the electronic charge density and the potential and the cutoff energy for expanding wave functions denoted by G_{MAX} and $R_{MT}K_{MAX}$ are chose 8 and 14 respectively [33]. By choosing mesh 4 × 10 × 10, 200 K-points were generated in the first Brillouin zone. The separating energy is 8 Ry, and the inter-atomic forces were minimized below 1.0 mRy/a.u.

3. Results and Discussion

Here is another look at MnAs properties, which is to create a nanosheet in line with (111) direction, with respect to Miller indices, with potential benefits to use in the industry of nano-electronic devices. Nano industry and science is a well-known and very interesting field [34-51]. With three non-collinear points that specify a plane, one can cut the crystal in the desired directions. If we consider these points on the crystal axes, then the plane can be obtained by specifying the coordinates of these points in terms of the lattice constants (a, b, c), so we study the nanosheet and find usage for this material as a magnetic metal in the electronics industry. Figure 1 shows the two-dimensional nanosheet MnAs in the NiAs phase along (111) direction.

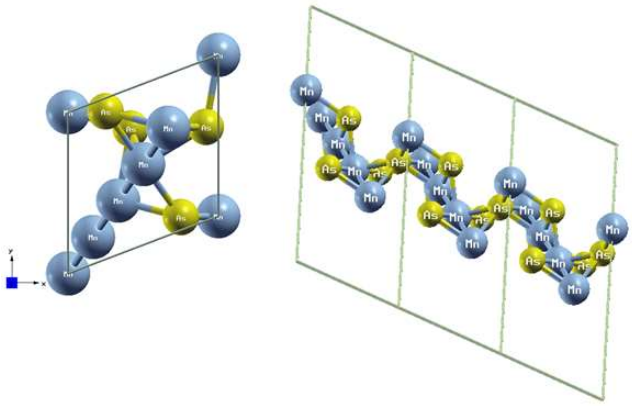

Fig. 1. Two views of MnAs nanosheet (111).

By creating a surface (111) from the bulk structure of MnAs, and in order to make more symmetries in the crystal, our space group is changed from a simple cubic (P) to a 47_Pmmm space group leading to 8 symmetries in the crystal in the k space. The nanosheet's primitive cell (111) consists of 5 Mn atoms and 4 As atoms located in nine different positions. In this case, the bond length of the Mn-As and Mn-Mn bonds was found to be 2.57Å and 2.85Å respectively. In the primitive cell (Fig. 1), each As atom is surrounded by three Mn atoms, and the Mn atoms themselves are bonded with 4 As and 2 Mn atoms (6 bonds). Using this information, our nano-structure was constructed and then we attempted to minimize the force between atoms. With these interpretations of the structural properties of crystals, we now look at the electronic and magnetic properties.

3.1 Study of electrical and magnetic properties

Figure 2 shows the density of states curve of the MnAs in bulk and in monolayer (111) phases. Our calculations are of spin-polarization type, which gives us accurate information about the magnetic and electronic properties of the crystal.

As it is seen, at both spins up and down, the electronic states cut the Fermi surface of the bulk MnAs, and have a very small spin polarization of about 10%. Most of the magnetic behavior of this compound is observed near the Fermi surface, which is what we expect from the NiAs phase. It is noteworthy that the major contribution to the density of states in the Fermi range belongs to the half-filled d-orbital of the Mn atom.

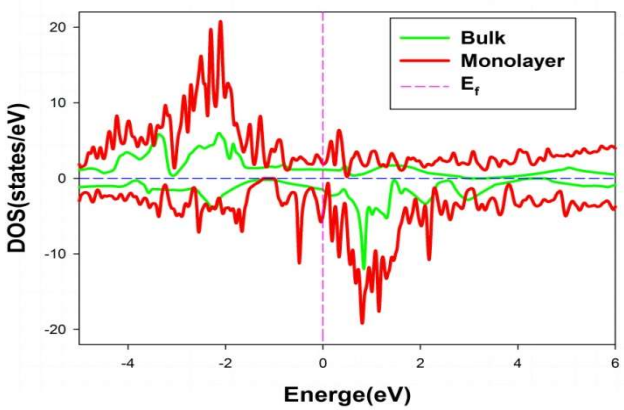

Fig. 2. The density of states of the nanosheet (111) in spin up and down.

In the monolayer, as shown in Figure 2, the density of states curve cut the Fermi surface at both spins up and down, so there are electronic states at the Fermi surface, i.e., this crystal is a conductor. The figure also shows that the graph is not symmetric for up and down spin states, especially around the Fermi surface, which means that the crystal is a magnetic metal. In this crystal, the total magnetic moment is 19.6 μ_B, which is very strong. The strongest effect to create such strong magnetization in the crystal is related to Mn atoms with magnetization of about 3.7 μ_B for each of them, and the other four atoms, As atoms, have smaller magnetic moments of approximately 0.15 μ_B. The remarkable point for the nanosheet (111) of crystalline MnAs is that the crystal which is a metal with low magnetization, and a low metallic property has turned into a good conductor of high magnetization. That is, by cutting the bulk crystal along (111) direction, we turned a half-metal into a conductor which can be useful for the industry of nano-electronic components.

To further study the electronic properties of the nanosheet (111) and the reason why it becomes a metal, we investigate the density of states curves of the Mn and As atoms and the partial density of states of each atom. Figure 3 shows the electronic density of states of the atoms Mn and As in the crystal's primitive cell compared to the total graph of the crystal in up and down states.

Fig.3a shows the density of states diagram of the Mn and As atoms in comparison with total states at spin up. As is evident in the figure, the most effect below the Fermi surface, and especially in the valence band, is related to the Mn atoms, while the As atom is far less effective. The maximum effect of the Mn atom's DOS is related to the energies of -4 eV to -2 eV. However, in the conduction band above and near the Fermi surface, the effects of the two atoms in the crystal are approximately equal.

In Fig.3b, we see that the maximum effect around the Fermi surface, particularly in the conduction band, belongs to Mn atoms, while the As atom has far less influence.

We can even state that As has almost no effect at the Fermi level compared to Mn. However, in the conduction band above the

Fermi surface, and in the valence band below the Fermi surface, the effect of the two atoms in the crystal is approximately the same.

3.2 Optical Properties

The dielectric tensor is used to investigate the crystal response to electromagnetic fields in different directions. Figure 4 illustrates the diagrams of the real and imaginary parts of the dielectric function in the x and z directions. The x-direction means the state where the light is irradiated to the (111) MnAs monolayer nanostructure in its plane while the z-axis direction is considered to be perpendicular to it. The peaks of the real part of the dielectric function are the material response to the incident photon. It can be seen that for both the x and z directions, the static value of the dielectric function tends to infinity. Moreover, this compound has long peaks in both directions in the IR region, and the transitions are the intraband type, indicating the metallic behavior of the structure in both directions. As the energy of the incident photon increases in the x direction, its first peak is observed in the IR region at the energy of 0.5 eV. Additionally, its highest peak is in the same area and at an energy of 1.5 eV. By increasing the incident light energy, the intensity of the peaks in the visible light region decreases, and a further decrease can be detected in the ultraviolet region. The graph becomes negative in the range of 0.6 eV to 0.8 eV, preparing the ground for metamaterial behavior. The presence of two roots around 0.6 eV to 0.8 eV can be a sign of the formation of Plasmon oscillations, but the material response in the z direction is higher than that of the x direction. In addition, the highest peak for both directions is observed in the visible light region and at the energy of 0.2 eV. The value of the real part of the dielectric function becomes less than 1 after the energy of 6 eV, so insulator and transparent behavior is expected for this compound.

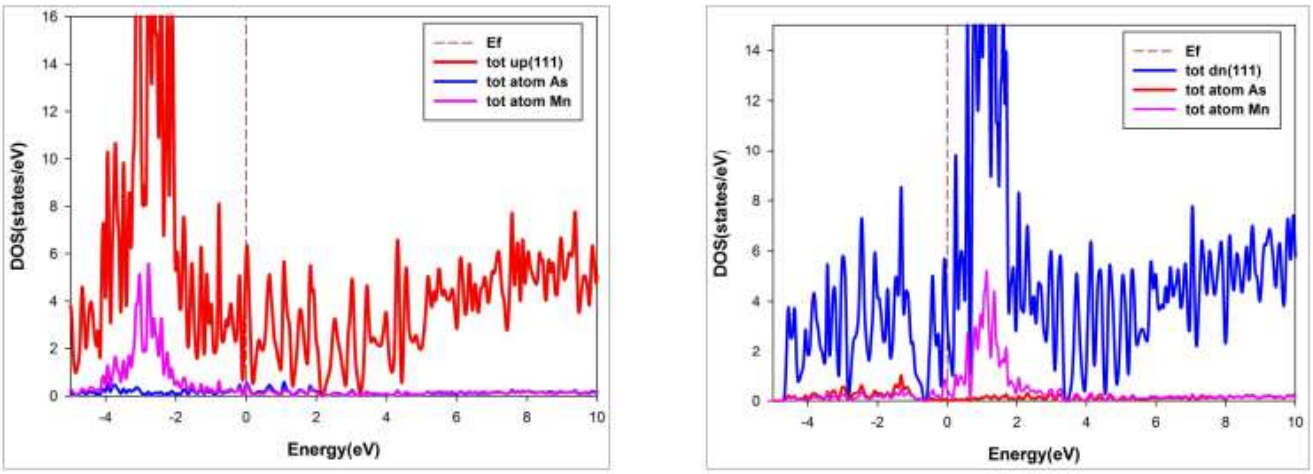

Fig. 3. The electronic density of states of the crystal's atoms for spins up (a), and down (b).

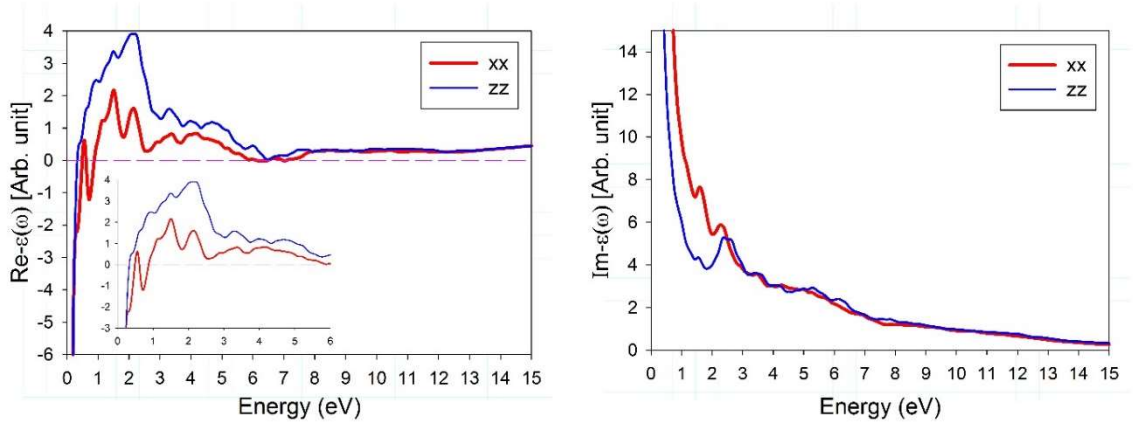

Fig. 4. Diagrams of real and imaginary parts in two symmetrical directions of x and z.

In Figure 4, the imaginary part of the dielectric function has also been shown for the two mentioned directions, and each peak of this electron diagram represents a transition from filled levels to empty ones. The diagram shows that this compound has long peaks in the IR region in the x and z directions, and the transitions are the intraband type, with both directions exhibiting metallic behavior. Calculations provide that there is no significant peak in both directions after the peaks of IR and visible light regions at the energies higher than 7 eV, so for the material behaves transparently both directions and above 7 eV.

Figure 5 displays the Eloss function spectra. The main peaks of this function for both x and z directions occurred at the energies higher than 13 eV. Therefore, this compound can be used in the IR, visible and UV regions with the lowest spectrum of energy loss in optical applications.

The summary of the electronic results can be seen in Figure 6 (right side), that is, optical conductivity. As a result of absorbing energy in the optical spectrum, the electrons of the bands of each material can gain energy and go to higher bands (unfilled) to cause conductivity. This diagram contains important information about the electronic structure of the material. Figure 7 illustrates the structure conductivity in terms of the incident photon energy in the x and z directions. The previous statements in the infrared region is emphasized again in the x and z directions. In the range of 0.5 eV, a sharp drop in conductivity is observed, which is due to the reduction of metal Plasmon oscillations in this range. However, the highest conductivity peaks are observed in the energy range from 5 eV to 6 eV, in which the conductivity peak occurs. By increasing the incident photon energy, the amount of this conductivity declines, and fewer electrons participate in the conductivity to reach a fixed saturation level.

In Figure 7 (left side), the real part of the refractive index, n(ω), of this compound is displayed in the x and z directions.

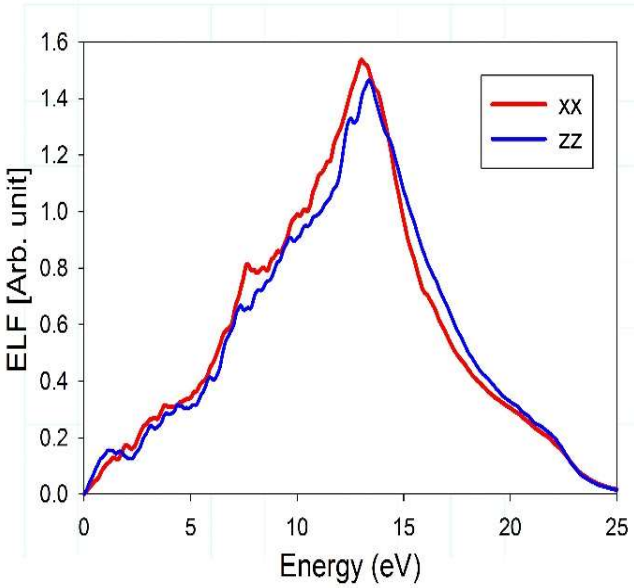

Fig. 5. Spectrum of the energy loss function for two directions of x and z.

As mentioned before, due to the metallic nature of this compound, its refractive index is large in static state in both directions. In all the IR and UV regions, the value of the real part of the refractive index faces almost little changes, and a sharp drop can be witnessed for these graphs. In both directions, the value of the refractive index becomes less than one from the energy of 6 eV onwards, indicating the superluminal phenomenon. From this energy onwards, the phase speed of light in this material becomes greater than the speed of light in vacuum.

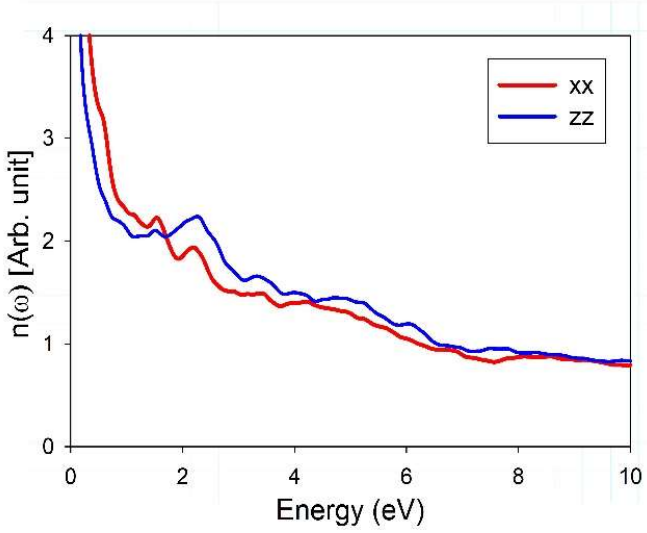

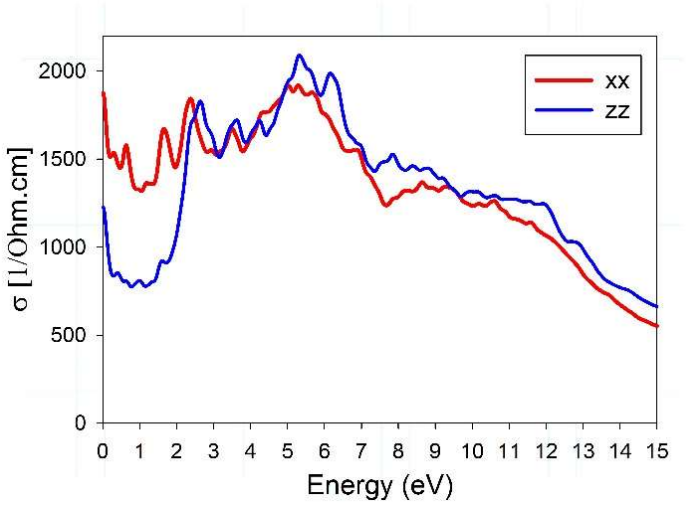

Fig. 6. Electrical conductivity diagram and real part of refractive index.

4. Conclusion

In this work, we studied the structural, electronic and magnetic properties of nanosheet MnAs (111) and compared them with the bulk case. This nanosheet can be advantageous in the industry of nano-electronic devices or other applications. In terms of structural properties, the material has become a nanosheet with a thickness of about 5 Å and is completely different from its bulk. The density of states curve cut the Fermi surface states, so we have electronic state at the Fermi surface, which means that our crystal is conductive. Also, we found that the graph for the spins up and down is different, especially around the Fermi surface suggesting a magnetic metal. In this crystal, the total magnetic moment is equal to 19.6a.u, whose magnetization is much stronger than the bulk state. The notable point in the nanosheet (111) of crystalline MnAs is that the crystal with half-metallic properties and lower magnetization and metallic property has become a good conductor of high magnetization. The major effect on the increasing magnetic property in MnAs (111) crystal is due to Mn. Interestingly, in spin up, the highest electronic state of Mn is in the valence region, and in spin down it is near the Fermi surface and the conduction region. The highest response is seen in the visible light region for both x and z directions, although the first peak is observed in the x direction in the IR region and Plasmon fluctuations can be seen in this region. At low energies, especially in the IR and visible light regions, the energy loss is low, and the peak of the energy loss is at higher energies than the infrared region. The transitions are the intraband type in the static state of the material in both directions, revealing its metallic properties, which is confirmed by the large refractive index in this area.

References

[1] K.Ono , J.Okabayashi, Mizuguchi, Fabrication, magnetic properties, and electronic structures of nanoscale zinc-blende MnAs dots (invited), Journal of applied physics, 91 (2002) 8088-8092.

[2] H. Akinaga, T. Manago, Shirai, Material Design of Half-Metallic Zinc-Blende CrAs and the Synthesis by Molecular-Beam EpitaxyJpn, Journal of applied physics,, Part2 39 (2000) 1118.

[3] R.J. SoulenJr, JM. Byers, MS. Osofsky, B. Nadgorny, Measuring the spin polarization of a metal with a superconducting point contact, Science, 2;282 (5386) (1998) 85-8.

[4] L. Makinistian, Measuring the spin polarization of a metal with a superconducting point contact" Physics Review. B 87 (2013) 220402.

[5] H. Lashgari, MR. Abolhassani, A. Boochani, E. Sartipi, R. Taghavi-Mendi, A. Ghaderi, Study of Pressure Effects on the Elastic Stability and Optical Treatment of Co2VAl using GGA+U" Indian Journal Physics, 90 (2016) 909-916.

[6] A. Boochani, M. Jamal, M. Shahrokhi, B. Nowrozi,M. B. Gholivand, Jabbar Khodadadi, Ti2VGe Heuslerene: theoretical prediction of a novel 2D material, ournal of Materials Chemistry, 10 (2019) 13559-13572.

[7] L. Bainsla, Suresh "Growth, structural, and magnetic properties of single-crystal full-Heusler Co2TiGe thin films" KG Curr Appl Phys, 121, 16:68 (2016).

[8] I. Galanakis, K. Özdoğan, and E. Şaşıoğlu, Ab initio electronic and magnetic properties of half-metallic NiCrSi and NiMnSi Heusler alloys, The role of defects and interfaces" Journal of Applied Physics, 104(8) (2009).

[9] L. Bainsla and K. G. Suresh, Equiatomic quaternary Heusler alloys: A material perspective for spintronic applications, Apply Physics Review 3(3) (2016).

[10] I. Galanakis, S. Ostanin, M. Alouani, H. Dreysse, J. Will, Theoretical study of magnetic properties and x-ray magnetic circular dichroism of the ordered Fe0.5Pd0.5 alloy 1(2000) 599.

[11] R. Groot, F. Mueller, P. Engen, van, K.H. Buschow, New class of materials: half-metallic ferromagnets, Physical Review Letters,50 (1983) 2024.

[12] I. Rungger and S. Sanvito, Ab initio study of the magnetostructural properties of MnAs, Physics Review. B 74, (2006) 024429.

[13] J. Mira, F. Rivadulla, J. Rivas, A. Fond ado, T. Guidi, R. Carciofi, F. Carsughi, P. G. Radaelli, and J. B. Goodenough Structural Transformation Induced by Magnetic Field and "Colossal-Like" Magnetoresistance Response above 313 K in MnAs" Physics Review Letter. 90 (2003) 097203.

[14] H. Wada and Y. Tanabe, Giant magnetocaloric effect of MnAs1−xSbx, Physics Review Letter. 79 (2001) 3302.

[15] A. K. Das, C. Pampuch, A. Ney, T. Hesjedal, L. Däweritz, R. Koch, and K. H. Ploog, Ferromagnetism of MnAs Studied by Heteroepitaxial Films on GaAs(001), Physics Review Letter. 91 (2003) 087203.

[16] H. Yamaguchi, A. K. Das, A. Ney, T. Hesjedal, C. Pampuch, D. M. Schaadt, and R. Koch "From ferro- to antiferromagnetism via exchange-striction of MnAs/GaAs (001), Euro physics Letters, 72(2005) 479.

[17] F. Iikawa, M. Brasil, C. Adriano, O. D. D. Couto, C. Giles,P. V. Santos, L. Däweritz, I. Rungger, and S. Sanvito, Phys, Lattice Distortion Effects on the Magnetostructural Phase Transition of MnAs, Review Letter. 95(2005) 077203.

[18] C. P. Bean and D. S. Rodbell" Magnetic Disorder as a First-Order Phase Transformation" Phys. Rev. 126, 104 (1962).

[19] C. Guillaud, J "Les points de transformation des composés définis MnAs, MnBi en relation avec un mechanism probable antiferromagnetism" Journal de Physique et le Radium, 12(1951) 223.

[20] R. H. Wilson and J. S. Kasper, The crystal structure of MnAs above 40°C, Acta Crystallographic. 17(1964) 95.

[21] G. E. Bacon and R. Street, Giant magnetoelastic response in MnAs" Nature _London; 175(1955) 518.

[22] C. Kittel" Model of Exchange-Inversion Magnetization" Physics Review. 120(1960) 335.

[23] J. P. Singh, J. Ji Mi, M. Kumar, J. Le Ik, H. Chae Keun, Unveiling the nature of adsorbed species onto the surface of MgO thin films during prolonged annealing, Journal Alloy Compound; 748 (2018) 355.

[24] B. Nourozi, A. Aminian, N. Fili, The Electronic and Optical properties of MgO mono-layer: based on GGA-Mbj, 677 (2018) 60.

[25] M. Stachowicz, M. Pietrzyk, D. Jarosz , P. Dluzewski, A. Kozanecki, ZnO/(Zn)MgO polar and nonpolar superlattices Surf Coat Technol, Journal of Applied Physics 35 (2018) 45.

[26] TS. Duffy, RJ.Hemley, H. Mao, Equation of state and shear strength at multimegabar pressures: Magnesium oxide to 227 GPa, Physics Review Letter, 74 (1995) 1371.

[27] W. Park, C.Yi , H. Jang, Growth and structural analysis of metalorganic chemical vapor deposited (11$\bar{2}$0) MgxZn1−xO (0<x<0.33) films on (01$\bar{1}$2) R-plane Al2O3 Substrates" Metalorganic. Apply Physics Letter 79 (2001)2022.

[28] L.C. Xu, R. Wang, M. Miao, Wei, Two-dimensional Dirac carbon allotropes from graphene, Nanoscale, 6 (2014) 1113.

[29] S. Cahangirov, M. Topsakal, E. Akturk, H. Sahin,S. Ciraci , Two- and One-Dimensional Honeycomb Structures of Silicon and Germanium" Phys Rev Lett; 102 (2009) 236804.

[30] X. Zhou, X. Dong, A. Oganov, Q. Zhu, Y. Tian , H. Wang, Semimetallic Two-Dimensional Boron Allotrope with Massless Dirac Fermions, Physics Review Letter, 112 (2014) 085502.

[31] K. S. P. Blaha, G. Madsen, D. Kvasnicka, J. Luitz, "WIEN2k, An Augmented Plane Waveplus Local Orbitals Program for Calculating Crystal Properties, Technical University of Vienna (2018).

[32] W. Kohn, and L. J. Sham, Self-Consistent Equations Including Exchange and Correlation Effects, Physical Review 140(1965) A1133-A1138.

[33] K. Bruke. J. P. Perdew, Int. J. Quant., Generalized gradient approximation for the exchange-correlation hole of a many-electron system, Physical Review, B 54 (1996).

Program for Calculating Crystal Properties, Technical University of Vienna (2018).

[34] A. K. O. Aldulaim, N. M. Hameed, T. A. Hamza, A. S. Abed, The antibacterial characteristics of fluorescent carbon nanoparticles modified silicone denture soft liner. *J. Nanostruct.,* 12 (2022) 774-781. doi:10.22052/JNS.2022.04.001.

[35] M. Y. Saleh, A.K.O. Aldulaimi, S.M. Saeed, A.H. Adhab, TiFe2O4@SiO2–SO3H: A novel and effective catalyst for esterification reaction , *Heliyon*, 4 (2024) https://doi.org/10.1016/j.heliyon.2024.e26286

[36] F. Arjomandi Rad, J. Talat Mehrabad, E. Dargahi Maleki, Synthesis and characterization of Gabapentin-Zn2 Al-LDH nanohybrid and investigation of its drug release and biocompatibility properties on a laboratory scale, J. Chem. Lett. 5 (2024). 10.22034/jchemlett.2024.442139.1157

[37] P. O. Ameh, Removal of Methylene Blue from Aqueous Solution using Nano Metal Oxide Prepared from Local Nigerian Hen Egg Shell: DFT And Experimental Study, *Chem. Rev. Lett.* 6 (2023) 29-43. 10.22034/crl.2023.328721.1155

[38] E. Vessally, M.R. Ilghami, M. Abbasian, Investigation the Capability of Doped Graphene Nanostructure in Magnesium and Barium Batteries with Quantum Calculations, *Chem. Res. Technol.* 1 (2024). 10.2234/chemrestec.2024.436837.1007.

[39] B. Baghernejad, F. Nuhi, A new approach to the facile synthesis of 1,8-dioxooctahydroxanthene using nano-TiO2/ CNT as an efficient catalyst, *Chem. Rev. Lett.* 6 (2022) 268-277. 10.22034/crl.2022.340828.1166

[40] P. O. Ameh, Synthesized iron oxide nanoparticles from Acacia nilotica leaves for the sequestration of some heavy metal ions in aqueous solutions, *J. Chem. Lett.* 4 (2023) 38-51. 10.22034/jchemlett.2023.360137.1083.

[41] H. Ashassi-Sorkhabi, A. Kazempour, J. Mostafaei, E. Asghari, Impact of ultrasound frequency on the corrosion resistance of electroless nickel-phosphorus-nanodiamond plating, *Chem. Rev. Lett.* 6 (2022) 187-192. 10.22034/crl.2022.345098.1169

[42] Milad. Sheydaei, M. Edraki, Poly(butylene trisulfide)/CNT nanocomposites: synthesis and effect of CNT content on thermal properties, *J. Chem. Lett.* 3 (2022) 159-163. 10.22034/jchemlett.2023.380990.1101.

[43] B. Ghanavati, A. Bozorgian, J. Ghanavati, Removal of Copper (II) Ions from the Effluent by Carbon Nanotubes Modified with Tetrahydrofuran, *Chem. Rev. Lett.* 6 (2022) 68-75. 10.22034/crl.2022.326950.1152

[44] M. Sheydaei, M. Edraki, Vinyl ester/C-MMT nanocomposites: investigation of mechanical and antimicrobial properties, *J. Chem. Lett.* 3 (2022) 95-98. 10.22034/jchemlett.2022.350678.1074.

[45] M. Sheydaei, S. Shahbazi-Ganjgah, E. Alinia-Ahandani, M. Sheidaie, M. Edraki, An overview of the use of plants, polymers and nanoparticles as antibacterial materials, *Chem. Rev. Lett.* 6 (2022) 207-216. 10.22034/crl.2022.343015.1168

[46] P. R. A. Selvan, M. Praveendaniel, Synthesis and Application of TiO2-Phosphomolybdic acid nanocomposite, *J. Chem. Lett.* 4 (2023) 10.22034/jchemlett.2023.395693.1114**.**

[47] S. Arabi, Adsorption of Orange 3R by chitosan modified montmorillonite nanocomposite, *Chem. Rev. Lett.* 6 (2023) 55-65. 10.22034/crl.2023.387842.1208.

[48] B. Mohammadi, M. R. Jalali Sarvestani, A Comparative Computational Investigation on Amantadine Adsorption on the Surfaces of Pristine, C-, Si-, and Ga-doped Aluminum Nitride Nanosheets, *J. Chem. Lett.* 4 (2023) 66-70. 10.22034/jchemlett.2023.388369.1107

[49] G. Lavanya, T. Suvarna, C.P. Vardhani, Structural and Optical Properties of (MgZnO/rGO) Nanocomposites, J. Chem. Lett. 4 (2023) 136-147. 10.22034/jchemlett.2023.396420.1116.

[50] C.-Y. Hsu, A. Yadav, S. M. Mohealdeen, Y. A. Abdulsayed, A. H. Adhab, S. Sharma, et al. Computational quantum mechanical investigation of the functionalized AlN nanotube as the smart carriers for levodopa drug delivery: a DFT analysis, Bulletin of Materials Science, 47 (2024) 1-8.

[51] B. Ajdari, S. A. Vahed, Fullerene (C20) as a sensing material for electrochemical detection of Nortriptyline: A theoretical study, *J. Chem. Lett.* 3 (2022) 164-168.10.22034/jchemlett.2023.385007.1104